Optimization of annealing conditions for Ag/p–GaN ohmic contacts

Sai Pan[1] · Youming Lu[1] · Zhibin Liang[1] · Chaojun Xu[1] · Danfeng Pan[2] · Yugang Zhou[1] · Rong Zhang[1] · Youdou Zheng[1]

Abstract

The electrical and optical properties of Ag/p–GaN contacts have been investigated as a function of the annealing temperature, oxygen concentration, and annealing time. Specific contact resistance (ρ_c) values as low as 1.2×10^{-4} $\Omega \cdot cm^2$ were obtained from the Ag/p–GaN contact annealed at 400 °C for 60 s in ambient O_2/N_2 (1:10). We found that the participation of oxygen improves the formation of ohmic contacts. Oxygen might remove the H in Mg–H complexes to activate the Mg acceptors and enhance Ga out-diffusion to form an Ag–Ga solid solution. We also found that the reflectivity of the Ag layer decreases with increasing annealing temperature in the O_2-containing ambient environment. Thus, an optimal annealing condition of Ag/p–GaN for blue and green LEDs is suggested based on these results. We also used the suggested annealing conditions to form ohmic contacts on DUV LEDs and achieved good electrical performance. The forward voltages of UVC LEDs fabricated with annealed Ag contacts were 6.60 V (7.66 V) at a 40 mA (100 mA) injection current.

Keywords Ohmic contact · Ag · p-GaN · Rapid thermal annealing · Circular transmission line model

1 Introduction

Silver (Ag) has a high reflectivity in the visible spectrum and is a desirable p-type reflector for blue and green LEDs [1]. However, Ag can agglomerate during annealing, leading to degradation in electrical and optical properties. To overcome this problem, several research groups have investigated different multimetal contacts, such as Ir/Ag [2], Ni/Ag [3], Ni/Au/Ag [4], and transparent conductive oxide/Ag contacts, such as ITO/Ag [5], CIO/Ag [6], and ZIO/Ag [7]. In addition, different Ag alloys, such as Ag–Al [8], Ag–Cu [1], and Ag–Mg alloys [9], have been investigated as p-GaN contacts and have been proven to suppress agglomeration. Although the structures were thermally stable, their reflectance was lower than that of a pure Ag layer. Therefore, it is important to find a proper annealing condition to optimize the trade-off between the electrical and optical properties of pure Ag/p–GaN contacts to improve blue and green LED performance.
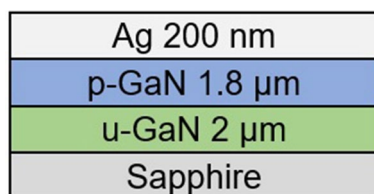
Ag contacts are also a candidate for ohmic contact in AlGaN-based deep-ultraviolet light-emitting diodes (DUV LEDs) [10]. Compared with low-pressure mercury lamps, ecofriendly and efficient DUV LEDs have a variety of important applications, including disinfection, sterilization, curing, photocatalysis, and phototherapy [11–14]. Because DUV light can kill SARS-CoV-2, which is the virus that causes COVID-19 infections, efforts to improve DUV LEDs are urgently needed [15]. The major factors limiting DUV LED efficiency are poor light extraction efficiency and low carrier injection efficiency. Both are closely related to the low p-type AlGaN conductivity and high p-type contact resistance [11]. In addition, less conductive p-AlGaN in a DUV LEDs leads to high operating voltages and high junction temperatures. At present, the p-GaN contact layer may become an alternative material to solve these problems despite its high absorption issue of p-GaN [16]. The formation of excellent metal–semiconductor ohmic contacts is important for the reliability and efficiency of DUV LEDs. Therefore, it is important to find proper annealing conditions to lower the Ag/p–GaN or Ag/p–AlGaN contact resistance for high-performance DUV LEDs.

✉ Yugang Zhou
  ygzhou@nju.edu.cn

1 Jiangsu Provincial Key Laboratory of Advanced Photonic and Electronic Materials and The School of Electronic Science and Engineering, Nanjing University, Nanjing 210023, China

2 Microfabrication and Integration Technology Center, Nanjing University, Nanjing 210023, China

Understanding the annealing mechanism of the ohmic contact is necessary to optimize the annealing conditions for Ag/p–GaN ohmic contacts. Jang et al. [17] found that annealing in ambient O_2 can promote the formation of ohmic contact at Ag/p–GaN interfaces. Song et al. [18] investigated the electrical and optical properties of Ag contacts as a function of the annealing temperature at only 330 °C and 530 °C. The stability of the Ag/p–GaN contact is sensitive to the contact and device processing parameters [4]. However, the effects of the annealing conditions, such as temperature, annealing time, and O_2:N_2 volume ratio, on the electrical properties have not been systematically investigated. In the work reported here, the influence of the O_2:N_2 volume ratio, annealing temperature, and annealing time on the Ag/p–GaN ohmic contact performance was studied. CTLM was used to measure the Ag/p–GaN contact resistance. An optimal annealing condition for Ag/p–GaN is suggested based on these results. In addition, we find that the participation of oxygen improves the formation of ohmic contacts. There have been many studies on the ohmic contact mechanism of Ag/p–GaN. We discuss the results of the present study with extensive reference to the results and conclusions of

the published literature and further confirm various mechanisms involved in Ag/p–GaN ohmic contact formation. In this work, the optimized annealing condition of Ag/p–GaN was applied to epitaxially AlGaN, which showed good I-V characteristics. The application of Ag in AlGaN-based DUV LEDs will be further studied soon.

2 Experimental Details

We prepared thick p-GaN epitaxial layers to measure specific contact resistance (ρ_c). These layers can be described as follows: a 1.8-µm-thick p-doped GaN layer was deposited on a 2 µm layer of undoped GaN (u-GaN) that had been grown on a sapphire substrate (Fig. 1). The hole concentration of the p-GaN was 8×10^{17} cm^{-3}.

The samples were first ultrasonically cleaned for 5 min in acetone and in isopropanol. Prior to placing them into the chamber for Ag deposition, all samples were dipped in $NH_3 \cdot H_2O$:H_2O_2:H_2O (1:1:5, 85 °C) solution for 10 min, then immersed in HCl solution (10%) for 10 min to remove any surface oxide layer or contamination. After the HCl treatment, Ag (200 nm) was deposited on p-GaN by electron beam evaporation. Then, CTLM patterns were created by standard photolithography and wet etching on the Ag/p–GaN side. The CTLM patterns had a constant inner radius (r_0) of 100 µm; the radii of the outer electrodes (R_n) varied from 106 to 136 µm. Figure 2 shows the contact pattern used in the CTLM method.

The samples were annealed at different temperatures in a rapid thermal annealer (AccuThermo AW 610, Allwin21 Corp.). The annealing times and O_2:N_2 volume ratios are

Fig. 1 Schematic of the epitaxial p-GaN in this work

Fig. 2 Schematic of the CTLM patterns in this work
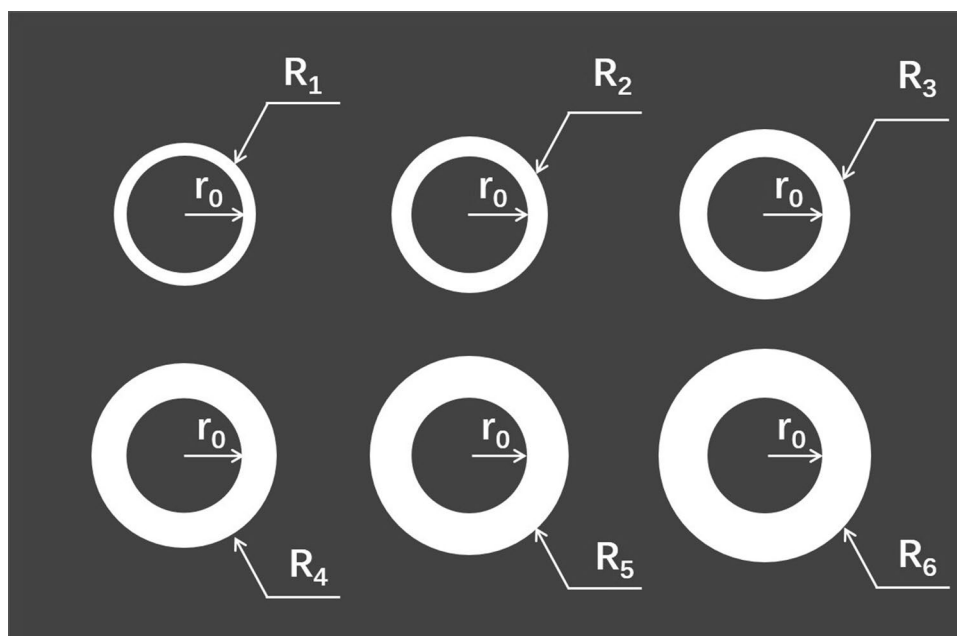
shown in Table 1. AccuThermo AW 610 allows the creation of recipes for automated control of the temperature and the process gas flows. We controlled the gas flows of commercial pure O_2, pure N_2 and O_2/N_2 mixed gas (2% O_2 volume percent), then mixed those gases to get the different O_2:N_2 volume ratios. A Keithley 2636B SourceMeter was used to measure current–voltage (*I–V*) properties. The morphology of Ag/p–GaN after annealing was observed by optical microscopy. A Lambda 950 ultraviolet–visible spectrophotometer (PerkinElmer) was used to measure the reflectivity of Ag deposited on double-polished sapphire under different annealing conditions. The incident light for reflectivity measurement originated from the sapphire side. We deposited a thin Ag metal layer (4 nm) on p-GaN by electron beam evaporation for X-ray photoelectron spectroscopy (XPS) measurement (PHI5000 Versaprobe, ULVAC-PHI, Inc.).

3 Results

Figure 3a shows typical *I–V* characteristics of Ag/p–GaN contacts that were annealed under different conditions. The diameter and spacing of the pattern used to obtain the *I–V* characteristics were 100 µm and 6 µm, respectively. This figure shows both typical ohmic contact with linear *I–V* behavior and nonohmic contact with nonlinear *I–V* behavior. Linear fits of R_{tot} vs. $\ln(R_n/r_0)$ were used to calculate contact

Table 1 Ag/p–GaN annealing process parameters

| Annealing temperature/°C	300/350/400/450
Annealing time/s	10/20/30/60/90
O_2:N_2 volume ratio/(O_2:N_2)	Pure O_2/1:1/1:10/1:50/1:100/1:300/1:700/ pure N_2

resistances for samples showing ohmic contact behavior. Figure 3b shows a typical linear fit of R_{tot} versus $\ln(R_n/r_0)$.

ρ_c of the Ag/p–GaN contacts after annealing at different temperatures and times are plotted in Fig. 4 with the O_2:N_2 volume ratio as the horizontal coordinate. In these graphs, ohmic contact data are represented by a solid line with solid shapes. Data from nonohmic contacts are represented by a dashed line with crosses.
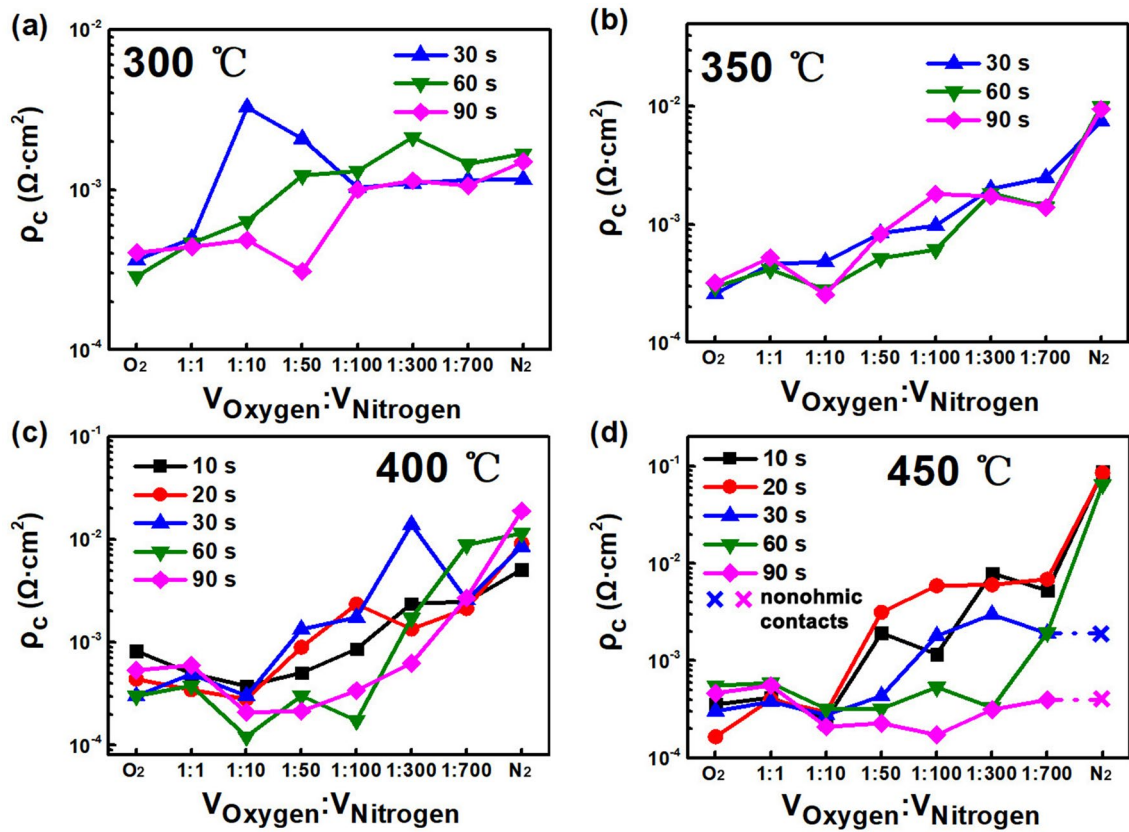
The 500X optical microscope images of Ag/p–GaN after annealing are presented in Fig. 5. The reflectance Ag on double-polished sapphire in the blue and green light ranges is shown in Fig. 6.

4 Discussion

As shown in Fig. 4, when the annealing temperature was 300 °C and the O_2:N_2 volume ratio was below 1:100, ρ_c changed only slightly with increasing annealing time. When the O_2:N_2 volume ratio was above 1:100, ρ_c decreased with increasing annealing time. When the annealing temperature was in the range from 350 to 450 °C and O_2:N_2 volume ratio was from pure N_2 to 1:10, ρ_c decreased with increasing O_2:N_2 volume ratio. The minimum value of ρ_c is 1.2×10^{-4} $\Omega \cdot cm^2$, which is achieved when the annealing temperature is 400 °C, the annealing time is 60 s, and the O_2:N_2 volume ratio is 1:10. It is clear that O_2 has a significant effect on ohmic contact. When the temperature is 450 °C and the O_2:N_2 volume ratio is 1:10, ρ_c is not sensitive to annealing time and ranges only between 2.1×10^{-4} and 3.2×10^{-4} $\Omega \cdot cm^2$. Additionally, when the annealing time is greater than 60 s, changing the O_2 concentration has little influence on the ohmic contact performance, and the Ag/p–GaN contact becomes nonohmic under a pure N_2 atmosphere.
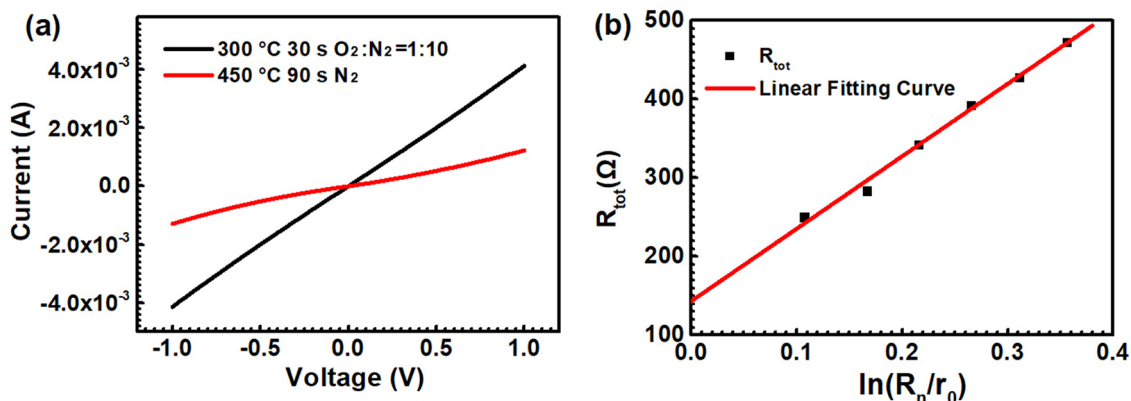
Fig. 3 **a** Current–voltage (*I–V*) characteristics of Ag/p–GaN contacts that were annealed under different conditions. **b** R_{tot} of the sample that was annealed at 300 °C for 30 s under ambient O_2 and N_2 (1:10)

Fig. 4 ρ_c of Ag/p–GaN contact in thick p-GaN after annealing for different times, under different O_2:N_2 volume ratios, and at different annealing temperatures: **a** 300 °C, **b** 350 °C, **c** 400 °C, **d** 450 °C
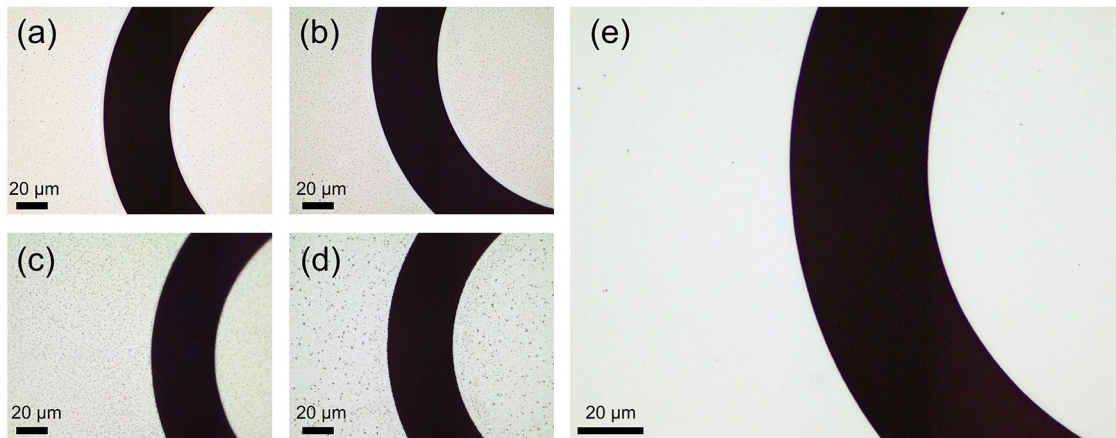
Fig. 5 500X optical microscope images of the samples annealed at **a** 300 °C for 90 s in ambient O_2:N_2 (1:50), **b** 350 °C for 90 s in ambient O_2:N_2 (1:10), **c** 400 °C for 60 s in ambient O_2:N_2 (1:100), **d** 450 °C for 60 s in ambient O_2:N_2 (1:300), and **e** 450 °C for 60 s in pure N_2

Based on the results, the participation of O_2 has an effect on ohmic contact formation with p-type GaN. The mechanism of ohmic contact formation on p-type GaN and the role of oxygen have been widely debated in the GaN community [19]. In p-GaN, Mg acceptors can be passivated by atomic hydrogen, reducing the free hole concentration [20]. Koide et al. [21] found that annealing in N_2/O_2 (3–100%) at ambient temperatures of 500~600 °C reduced both the ρ_c and sheet resistivity of p-GaN for in contact with Ni/Au. The hole concentration of p-GaN increased from 3.4×10^{17}
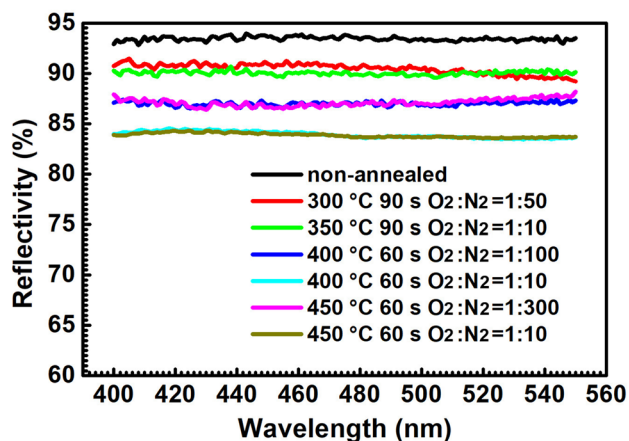
Fig. 6 Reflectivity of Ag on double-polished sapphire under blue and green light after annealing under different conditions

to 5.0×10^{17} cm^{-3}. They strongly believed that the reduced contact resistivity was caused by the increased hole concentration at the GaN surface. Because the hydrogen atoms of Mg-H complexes might be removed in O_2-containing ambient conditions, p-GaN with a higher acceptor concentration was formed. Hull et al. [22] showed that the resistivity of p-GaN decreased when annealed with intentionally incorporated O_2. The SIMS analysis data confirmed that O_2 enhances the out-diffusion of hydrogen from the p-GaN epitaxial layer. Wu et al. [23] also investigated the effect of O_2 on activating p-GaN by rapid thermal annealing. They confirmed the positive effect of O_2 in the thermal annealing of p-GaN. The process was related to the concentration of O_2, annealing time and temperature. However, the quantity of Mg-H that can be activated is limited, so optimization of ohmic contacts has a saturation effect. The results in our work followed this trend. Before the annealing process parameters reach the critical condition, the contact resistance will significantly decrease as the temperature, O_2:N_2 volume ratio, or annealing time increase. However, when the concentration of O_2, the annealing time, and/or the temperature was sufficiently high, the Mg-H activation effect was saturated and ρ_c no longer decreased.

For flip-chip LEDs, p-type ohmic contact with low contact resistivity and high reflectance is essential to enhance light extraction and reduce power consumption. When annealed, the agglomeration phenomenon of the Ag layer occurs, resulting in the degradation of electrical properties [24]. Although O_2 has a positive effect on Ag/p–GaN contacts, Ag agglomerates because of the participation of O_2 during the annealing process, resulting in reduced reflectivity of the Ag layer [1, 25]. Agglomeration of Ag generally leads to a lower optical output power. Hence, the thermal stability of Ag is closely related to the reliability of the LED. Sharma and Spitz deposited Ag films on quartz substrates

and annealed those samples in different atmospheres [26]. Hillocks formed on the surface of the Ag film after annealing, and further heating in ambient O_2 led to Ag agglomeration in the film. The formation of hillocks was attributed to the relaxation of thermal stress by diffusion creep. The surface self-diffusion of Ag atoms is enhanced by a factor of 100 in the presence of oxygen. Crocombette et al. [27] studied the binding energies of oxygen vacancies in Ag by density functional theory calculations using a plane wave basis set. When the oxygen atom is substituted for Ag, the energy of the oxygen-vacancy pair is lowest (-0.39 eV). Thus, the presence of oxygen greatly favors the formation of divacancies and enhances agglomeration. The surface of those samples is shown in the 500X optical microscope images in Fig. 5. Defects related Ag agglomeration was observed with the presence of O_2 and became worse when temperature and O_2:N_2 volume ratio increases. However, no Ag aggregation effect was observed in the pure N_2 atmosphere, even when the annealing temperature was as high as 450 °C, as shown in Fig. 5e. Similarly, de Monestrol et al. [28] annealed Ag films in Ar and O_2 atmospheres and found no agglomeration in Ar atmospheres. Therefore, the agglomeration of Ag is strongly dependent on the annealing temperature and is accelerated by O_2. We calibrated the reflectivity of the as-deposited Ag layer using the as-deposited Ag layer with 93% reflectivity in the visible range. The measured reflectivity at a wavelength of 450 nm was 91.0%, and 86.6% for the Ag layers annealed at 300 °C for 90 s under O_2:N_2 (1:50), and 450 °C for 60 s under O_2:N_2 (1:300), respectively. With an increase in annealing temperature, the reflectivity shows a decreasing trend. The sample annealed at 400 °C for 60 s under O_2:N_2 (1:100) produced a reflectance of 86.8% at 450 nm, whereas the sample annealed at 400 °C for 60 s under O_2:N_2 (1:10) had 84.2%. Oxygen promoted the agglomeration of Ag.

The interfacial reactions and changing of the binding energy are also very important for the formation of good Ag/p–GaN ohmic contacts, which have also been investigated in detail. Song and Seong [29] used Ag/SnO_2 as the highly transparent and low-resistance ohmic contact layer to p-GaN in 2004. They used XPS to characterize the chemical bonding state of Ga and Ag. The Ga $2p$ binding energy was shifted to the lower energy side by 0.36 eV after annealing. The binding energy shift indicates that the surface Fermi level moves closer to the valence band edge, reducing the Schottky barrier height. They attributed this phenomenon to the formation of a Ag–Ga solid solution near the Ag/p–GaN contact interface, resulting in deep acceptor-like Ga vacancies near the surface. Song et al. also observed this phenomenon in the other Ag-based ohmic contact layer to p-GaN [6, 18, 30]. The Ag–Ga solid solution theory has been accepted by other groups of researchers [1, 25, 31, 32]. In addition, Jang et al. [33] found that the peak of Ga $3d$ shifted toward a

lower binding energy by 0.4 eV in the O_2-annealed sample, while it shifted only 0.2 eV in the N_2-annealing sample. The intensity of the metallic Ga bond was stronger when the sample was annealed in ambient O_2. They believed that oxygen can improve Ga out-diffusion into Ag layers to form an Ag–Ga solid solution during annealing. This is also consistent with the reflectivity results from samples annealed at different O_2:N_2 volume ratios and temperatures, as discussed above (see Fig. 5). Jang et al. [17, 34] received good Ag-based ohmic contact with p-GaN by annealing the samples in ambient O_2. Their results indicated that Ga out-diffusion was enhanced when O_2 participated in the annealing process. Chen et al. [35] found that Ag can form ohmic contacts at annealing temperatures as low as 200 °C in ambient air. The results of Kim et al. indicate that a higher annealing temperature is needed to promote the formation of an Ag–Ga solid solution without excessive oxygen. Figure 7 shows the XPS spectra of Ga 3*d* core levels for thin Ag contacts after annealing at 400 °C for 60 s under different atmospheres. The Ga 3*d* core level for the sample annealed under O_2:N_2 (1:700) shifts toward the lower binding energy side by 0.04 eV compared to that of the sample annealed under pure N_2. The shift was even larger to be 0.1 eV in the sample annealed under O_2:N_2 (1:10), agreeing well with the previously reported values. The relationship between ρ_c and annealing process parameters in this work could also confirm the promotional effect of O_2. When the annealing temperature is relatively low (300 °C), the promotional
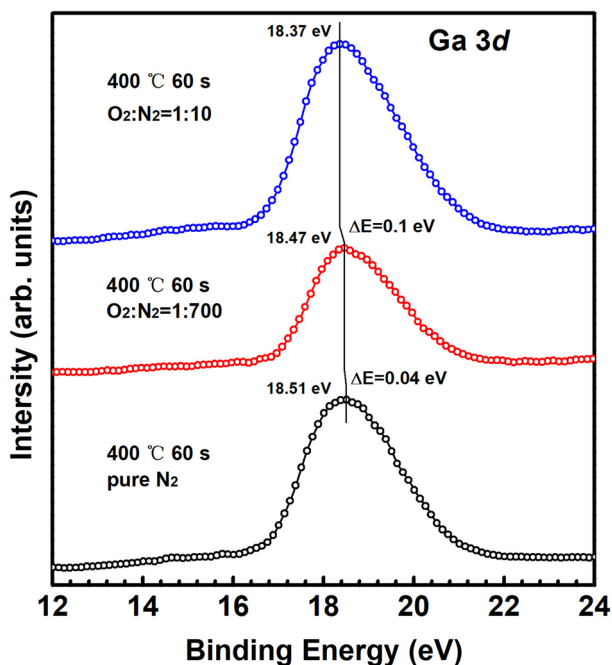
effect of O_2 is relatively slow. Therefore, increasing the annealing time and O_2 concentration can promote Mg activation and Ga diffusion, leading to a decrease in ρ_c. When the annealing temperature is relatively high (450 °C), the promotional effect of O_2 is relatively high. Therefore, even when the O_2:N_2 volume ratio is as low as 1:700, ρ_c can still reach 3.98×10^{-4} $\Omega \cdot cm^2$ when the annealing time is 90 s. In a pure N_2 atmosphere, neither Mg activation nor Ga diffusion is active. At the same time, high temperature causes an increase in N vacancies, leading to nonohmic behavior [23]. In conclusion, the influences of temperature, O_2:N_2 volume ratio, and annealing time on ρ_c are coupled. When the annealing temperature, time, and O_2:N_2 volume ratio are below the critical condition, the contact resistance will significantly decrease as the temperature, O_2:N_2 volume ratio, or annealing time increase. When the annealing condition crosses a critical border, a further increase in temperature, O_2:N_2 volume ratio, or annealing time will not significantly change the contact resistance.
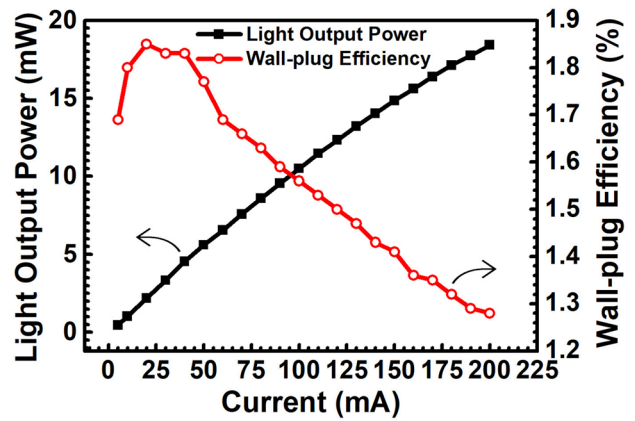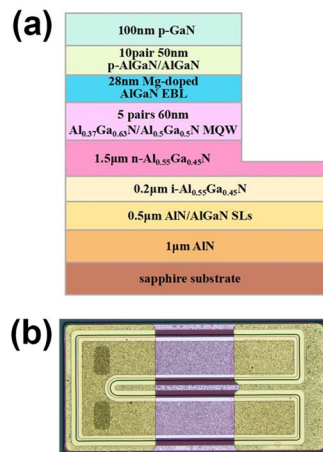
Even though O_2 has a positive effect on the Ag/p–GaN ohmic contact, the resistivity of p-GaN was increased at 700 °C in 10% O_2/90% N_2 when the activation time was longer [22]. Wu et al. [23] measured the SIMS depth profiles of the samples annealed at 750 °C and 850 °C in the same 20% O_2/80% N_2 because the resistivity of the sample annealed at 850 °C is higher than that annealed at 750 °C. They found that the concentration of hydrogen in the sample annealed at 850 °C was lower, while the concentration of oxygen was higher. Thus, they believed that oxygen also compensated the acceptors in p-GaN. In this work, when the annealing temperature is relatively low (300 °C and 350 °C), the promotional effect of O_2 is relatively slow. Therefore, pure O_2 and O_2:N_2 (1:1) can promote Mg activation and Ga diffusion, leading to a decrease in ρ_c. When the annealing temperature is relatively high (400 °C and 450 °C), the ρ_c of samples annealed under pure O_2 and O_2:N_2 (1:1) were larger than those annealed under O_2:N_2 (1:10). Because oxygen is a donor in p-GaN, the penetration of oxygen might compensate acceptors in p-GaN if the O_2 concentration, activation time and temperature are excessive. Therefore, the ρ_c increase when the samples annealed under high O_2 concentration atmosphere at high temperature.

By adjusting the annealing temperature, annealing time, and oxygen concentration, one can take advantage of the trade-off between electrical and optical properties for Ag/p–GaN. The p-type contact with low ρ_c and high reflectance is of particular importance to the development of high-efficiency flip-chip LEDs (FC-LEDs). When the annealing temperature was 300 °C and 350 °C, the ρ_c were not low enough to realize the highly efficient FC-LEDs. When the annealing temperature was 400 °C and 450 °C, ρ_c is low enough for the highly efficient FC-LEDs. Even the surface morphology of the Ag was not quite smooth, after annealed

Fig. 7 X-ray photoelectron spectroscopy (XPS) Ga 3*d* core level spectra obtained from Ag/*p*-GaN after annealing at 400 °C for 60 s under different atmospheres

at 400 °C and 450 °C (see Fig. 5). The reflectivity of samples annealed at 400 °C, 450 °C for 60 s under O_2:N_2 (1:10) at 450 nm was still 84.2%, and 84.0%, respectively (see Fig. 6). Thus, 400–450 °C could be the appropriate annealing temperature. O_2 could improve the information of ohmic contact, the O_2:N_2 volume ratio (1:10–1:50) was choosing as annealing atmosphere. There may be risk to ensure repeatable optimum contact resistance if the annealing time is too short. Thus, for blue and green LEDs, we suggest that the annealing temperature should be 400–450 °C, the O_2:N_2 volume ratio should be 1:10–1:50, and the annealing time should be 60–90 s. In this work, under this process window condition, ρ_c is as low as 1.2×10^{-4} $\Omega \cdot cm^2$. This process window is large enough to ensure the stability, repeatability, and operability of the production process.

We also tried the suggested annealing condition for ohmic contacts on DUV LEDs, whose epitaxial structure is shown in Fig. 8a. We deposited 200 nm Ag on the p-GaN of AlGaN-based DUV LEDs, and the Ag/p–GaN was annealed at 450 °C for 60 s under ambient O_2 and N_2 (0.6:10). The chip size dimension for the DUV LEDs is 250 μm × 500 μm, as shown in Fig. 8b. The *I–V* characteristics of DUV LEDs with annealed Ag electrodes are plotted in Fig. 8c. The inset shows the linear, ohmic *I–V* characteristics of the Ag/p–GaN contacts after annealing. Under a 40 mA (100 mA) injection current, the forward voltage of the DUV LEDs is 6.60 V (7.66 V). Figure 9 shows the light output power (LOP) and wall-plug efficiency (WPE) as a function of injection current for the DUV-LED measured under DC conditions. The LOP and EQE were 4.54 mW and 1.83% at the injection current of 40 mA and 10.5 mW and 1.56% at the injection current of 100 mA, respectively. The results indicated that the optimized annealing conditions can also be applied to DUV LEDs. Further optimization may be needed for Ag contacts on DUV LEDs and will be investigated in future work.
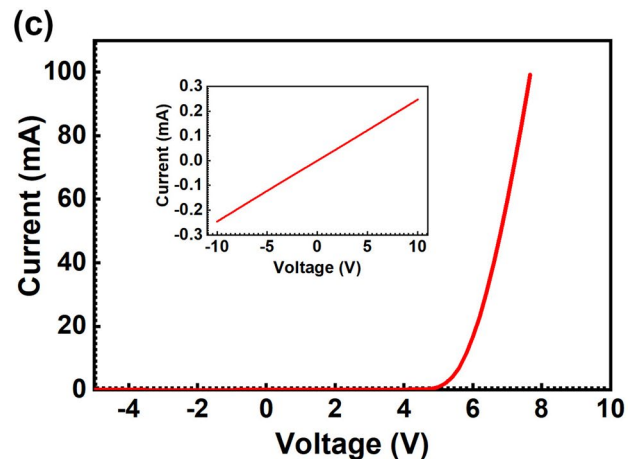

Fig. 9 Light output power (LOP) and wall-plug efficiency (WPE) as a function of injection current for the DUV-LED during DC operation

5 Conclusions

We investigated the optimal annealing conditions of Ag/p–GaN using the circular transmission line model (CTLM). The annealing temperature, oxygen concentration, and annealing time were found to jointly influence the Ag/p–GaN ohmic contact. O_2 was found to be indispensable for forming good Ag/p–GaN ohmic contacts. A possible mechanism is that O_2 combines with H in Mg-H complexes to activate Mg acceptors and improve Ga out-diffusion to Ag layers, forming an Ag–Ga solid solution. However, O_2 can enhance the agglomeration of Ag during the annealing process, which reduces reflectivity of the Ag layer. We suggest that the optimal Ag/p–GaN annealing condition is 400–450 °C for 60–90 s in O_2:N_2(1:10–1:50) for blue and green LEDs. Under these conditions, a value of ρ_c as low as 1.2×10^{-4} $\Omega \cdot cm^2$ can be achieved. The suggested annealing conditions can also be used for DUV LEDs. The forward

Fig. 8 **a** Schematic of the epitaxial structure details for the DUV LEDs of this study. **b** Photograph of the DUV LED test sample. **c** *I–V* characteristics of AlGaN-based DUV LEDs after annealing. The inset shows the *I–V* characteristics between two annealed Ag contacts on the surface of a DUV LED structure

voltage at a current of 40 mA (100 mA) for the DUV LEDs is 6.60 V (7.66 V).

References

1. J.-S. Kwon, J.-Y. Beak, N.-W. Kang, M. Hong, C. Lim, J. Im, S. Oh, B.-Y. Jeong, S. Cho, K.-K. Kim, J. Nanosci. Nanotechnol. **18**, 9 (2018)
2. K.-Y. Ban, H.-G. Hong, D.-Y. Noh, J.I. Sohn, D.-J. Kang, T.-Y. Seong, Mater. Sci. Eng. B **133**, 1–3 (2006)
3. X. Liu, N. Li, J. Hu, Y. Gao, R. Wang, S. Zhou, ECS J. Solid State Sci. Technol. **7**, 6 (2018)
4. D.L. Hibbard, S.P. Jung, C. Wang, D. Ullery, Y.S. Zhao, H.P. Lee, W. So, H. Liu, Appl. Phys. Lett. **83**, 2 (2003)
5. S. Kim, J.-H. Jang, J.-S. Lee, J. Electrochem. Soc. **154**, 11 (2007)
6. J.O. Song, J.S. Kwak, T.Y. Seong, Appl. Phys. Lett. **86**, 6 (2005)
7. L.-C. Chen, Y.-M. Ho, J. Phys. D-Appl. Phys. **40**, 21 (2007)
8. J.Y. Kim, S.I. Na, G.Y. Ha, M.K. Kwon, I.K. Park, J.H. Lim, S.J. Park, M.H. Kim, D. Choi, K. Min, Appl. Phys. Lett. **88**, 4 (2006)
9. Y.H. Song, J.H. Son, G.H. Jung, J.-L. Lee, Electrochem. Solid State Lett. **13**, 6 (2010)
10. N. Zhang, F.J. Xu, J. Lang, L.B. Wang, J.M. Wang, Y.H. Sun, B.Y. Liu, N. Xie, X.Z. Fang, X.L. Yang, X.N. Kang, X.Q. Wang, Z.X. Qin, W.K. Ge, B. Shen, Opt Express **29**, 2 (2021)
11. H. Amano, R. Collazo, C.D. Santi, S. Einfeldt, M. Funato, J. Glaab, S. Hagedorn, A. Hirano, H. Hirayama, H. Ishii, Y. Kashima, Y. Kawakami, R. Kirste, M. Kneissl, R. Martin, F. Mehnke, M. Meneghini, A. Ougazzaden, P.J. Parbrook, S. Rajan, P. Reddy, F. Römer, J. Ruschel, B. Sarkar, F. Scholz, L.J. Schowalter, P. Shields, Z. Sitar, L. Sulmoni, T. Wang, T. Wernicke, M. Weyers, B. Witzigmann, Y.-R. Wu, T. Wunderer, Y. Zhang, J. Phys. D Appl. Phys. **53**, 50 (2020)
12. J. Zhang, L. Chang, Y. Zheng, C. Chu, K. Tian, C. Fan, Y. Zhang, Z.-H. Zhang, Opt. Express **28**, 11 (2020)
13. T.H. Lee, T.H. Park, H.W. Shin, N. Maeda, M. Jo, H. Hirayama, B.-H. Kim, T.G. Kim, Adv. Opt. Mater. **8**, 2 (2020)
14. Q. Chen, H. Zhang, J. Dai, S. Zhang, S. Wang, J. He, R. Liang, Z.-H. Zhang, C. Chen, IEEE Photonics J. **10**, 4 (2018)
15. M.A. Khan, Y. Itokazu, N. Maeda, M. Jo, Y. Yamada, H. Hirayama, ACS Appl. Electron. Mater. **2**, 7 (2020)
16. K.-P. Chang, J.-Y. Jheng, S.-Y. Huang, W.-K. Wang, R.-H. Horng, D.-S. Wuu, Semicond. Sci. Technol. **35**, 10 (2020)
17. H.W. Jang, J.H. Son, J.-L. Lee, Appl. Phys. Lett. **90**, 1 (2007)
18. J.-O. Song, J.S. Kwak, Y. Park, T.-Y. Seong, Appl. Phys. Lett. **86**, 6 (2005)
19. G. Greco, F. Iucolano, F. Roccaforte, Appl. Surf. Sci. **383** (2016)
20. W. Götz, N.M. Johnson, J. Walker, D.P. Bour, R.A. Street, Appl. Phys. Lett. **68**, 5 (1996)
21. Y. Koide, T. Maeda, T. Kawakami, S. Fujita, T. Uemura, N. Shibata, M. Murakami, J. Electron. Mater. **28**, 3 (1999)
22. B.A. Hull, S.E. Mohney, H.S. Venugopalan, J.C. Ramer, Appl. Phys. Lett. **76**, 16 (2000)
23. L.L. Wu, D.G. Zhao, D.S. Jiang, P. Chen, L.C. Le, L. Li, Z.S. Liu, S.M. Zhang, J.J. Zhu, H. Wang, B.S. Zhang, H. Yang, Semicond. Sci. Technol. **27**, 8 (2012)
24. H.C. Kim, T.L. Alford, J. Appl. Phys. **94**, 8 (2003)
25. H. Kim, K.H. Baik, J. Cho, J.W. Lee, S. Yoon, H. Kim, S.-N. Lee, C. Sone, Y. Park, T.-Y. Seong, IEEE Photonics Technol. Lett. **19**, 5–8 (2007)
26. S.K. Sharma, J. Spitz, Thin Solid Films **65**, 3 (1980)
27. J.-P. Crocombette, H. de Monestrol, F. Willaime, Phys. Rev. B **66**, 2 (2002)
28. H. de Monestrol, L. Schmirgeld-Mignot, P.J.A. Molinàs-Mata, S. Poissonnet, G. Martin, Acta Mater. **49**, 9 (2001)
29. J.-O. Song, T.-Y. Seong, Appl. Phys. Lett. **85**, 26 (2004)
30. J.O. Song, W.K. Hong, Y. Park, J.S. Kwak, T.Y. Seong, Appl. Phys. Lett. **86**, 13 (2005)
31. J.H. Son, G.H. Jung, J.-L. Lee, Appl. Phys. Lett. **93**, 1 (2008)
32. W.-S. Yum, J.-W. Jeon, J.-S. Sung, T.-Y. Seong, Opt. Express **20**, 17 (2012)
33. H.W. Jang, S.Y. Kim, J.-L. Lee, J. Appl. Phys. **94**, 3 (2003)
34. H.W. Jang, J.H. Son, J.-L. Lee, J. Electrochem. Soc. **155**, 8 (2008)
35. I.C. Chen, Y.-D. Chen, C.-C. Hsieh, C.-H. Kuo, L.-C. Chang, J. Electrochem. Soc. **158**, 3 (2011)

Publisher's Note Springer Nature remains neutral with regard to jurisdictional claims in published maps and institutional affiliations.